Fractional Synchrosqueezing Transformation and Its Application in the Estimation of the Instantaneous Frequency of a Rolling Bearing

XIN LI[1,2], ZENGQIANG MA[1,3], SUYAN LIU[1,3], (Member, IEEE), AND FEIYU LU[3]

[1]State Key Laboratory of Mechanical Behavior and System Safety of Traffic Engineering Structures, Shijiazhuang Tiedao University, Shijiazhuang 050043, China
[2]School of Traffic and Transportation, Shijiazhuang Tiedao University, Shijiazhuang 050043, China
[3]School of Electrical and Electronic Engineering, Shijiazhuang Tiedao University, Shijiazhuang 050043, China

Corresponding author: Zengqiang Ma (mzqlunwen@126.com)

ABSTRACT The time-frequency energy distribution processed by a short-time Fourier transform can be compressed to the real instantaneous frequency by the synchrosqueezing transformation (SST), which improves the time-frequency energy concentration of the signal. However, there is a large error in the instantaneous frequency estimation of a multicomponent nonpure harmonic signal by the SST. Therefore, a method for determining the instantaneous frequency (IF) of a rolling bearing based on a fractional synchrosqueezing transformation (FRSST) is proposed. First, the theoretical derivation of the FRSST algorithm as a signal processing technique is given and the steps of the IF estimation are presented. Second, the main advantages of the proposed FRSST algorithm are proved. In the comparison of simulation signals, it is verified that the FRSST algorithm has a high time-frequency concentration, is non-fragile to the frequency modulation rate, has noise robustness and has nonsensitivity to the cross-frequency signal. Finally, the FRSST algorithm is applied to the IF estimation of a rolling bearing under rising speed and fluctuated speed, and is compared with the SST based on variational mode decomposition (VMD-SST), the generalized parametric SST (PSST) and polynomial chirplet transform (PCT). The test results show that the estimation error of IF based on the FRSST method is the least for a rolling bearing with the four fault types under rising speed. On average, the estimation error is 2.2180 Hz less than the corresponding error of the VMD-SST and 1.1862 Hz less than the corresponding error of the PSST method.

INDEX TERMS Fractional synchrosqueezing transformation, instantaneous frequency, noise robustness, rolling bearing.

I. INTRODUCTION

The rolling bearing is the key component of rotating machinery, which is widely used. Because the rolling bearing's working state directly affects the operational efficiency and service life of a mechanical system, it is of great significance to study its fault diagnosis [1]–[3]. Under the condition of variable speed, the key to the fault diagnosis of a rolling bearing is how to identify the IF effectively by the vibration signal [4]–[8]. As a result, methods that can obtain the IF information from

the vibration signal have attracted considerable attention in recent years.

The research on IF extraction is divided into two categories. The first category is order tracking which converts the nonstationary vibration signal into a stationary one. The most widely used methods include order features extraction [9], [10], order analysis [11], [12] and synchronous averaging [13], [14]. These methods usually require the installation of an additional key-phase device to measure the actual speed of the bearings, but it is difficult to implement when the installation of the device is inconvenient. The other category involves methods with no key-phase device

The associate editor coordinating the review of this manuscript and approving it for publication was Jinming Wen.

focused on the IF estimation that is mainly based on the phase demodulation [15]–[18] and time-frequency representation [19]–[23]. The former type of method demodulates the harmonic signal extracted from the rolling bearing vibration signals to obtain instantaneous phase information, but it can only obtain this information when the harmonics constantly exist in the rolling bearing vibration signal and have a sufficiently high energy level. However, in most practical cases such harmonics are very difficult to detect due to the existence of background noise and resonance [24]. The later type of method transforms the vibration signal into the time-frequency domain, so the instantaneous frequency information of a harmonic signal can be extracted by a ridge extraction algorithm and the noise can be effectively suppressed. Thus, the time-frequency representation method is often used for the rolling bearing systems with strong noise.

Time-frequency analysis is an important tool to analyze the instantaneous characteristic frequency of nonstationary signals. In this method, a one-dimensional frequency domain or time domain signal is mapped to a two-dimensional time-frequency domain plane, and the time-frequency distribution of the signals is obtained. Finally, the instantaneous characteristic frequency of each component signal is extracted in the time-frequency domain. Based on the above theory, a series of time-frequency analysis algorithms for instantaneous characteristic frequency extraction have emerged, such as the short-time Fourier transform (STFT) [25], Wigner-Ville distribution (WVD) [26], [27], and wavelet transform. These algorithms' main advantages and disadvantages are analyzed and discussed in many literatures and will not be described here. To improve the energy concentration, which is an important index to measure the effectiveness of the time-frequency analysis algorithm, the SST is introduced into the time-frequency analysis algorithm. In reference [28], the SST method based on wavelet transform is proposed to improve the energy concentration in the frequency's direction and support signal reconstruction, but the time-frequency resolution is low at high frequency. As an extension of the method, the SST method based on the STFT is proposed in [29]. Although the time-frequency resolution at high frequency is improved, the anti-noise capability is poor.

The SST can comprehensively describe the characteristics of a bearing fault signal frequency that changes over time, but the SST algorithm has two shortcomings. One shortcoming is that the accuracy is high only for the harmonic signal that has a constant instantaneous frequency; it is low when the instantaneous frequency changes dramatically. Second, in practical applications, the nonstationary bearing vibration signal usually contains multiple components that will appear simultaneously in the time domain; furthermore, the instantaneous frequency may overlap in the frequency domain or the instantaneous frequency difference of each component may be small. At this time, the most clear and real time-frequency information cannot be obtained by the SST algorithm [30]. Considering the nonlinear, strong noise and multicomponent characteristics of the rolling bearing vibration signal,

combined with the advantages of STFRFT algorithm, the FRSST combining the STFRFT and the SST is proposed to realize the instantaneous frequency estimation of a multi-component nonpure harmonic signal. The FRSST algorithm has strong noise robustness and can improve the estimation accuracy of the instantaneous fault frequency of a rolling bearing.

The main contributions of the paper are as follows: (i) the theoretical derivation of the FRSST algorithm as a signal processing technique is given and the steps of the IF estimation are presented. The FRSST can realize the instantaneous frequency extraction of a multicomponent signal with frequencies that cross or are close and can support signal reconstruction. (ii) According to the characteristics of the rolling bearing signal and the advantages of the FRSST, the FRSST algorithm is introduced into the IF estimation of a rolling bearing. This algorithm improves the energy concentration of the time-frequency distribution of a rolling bearing vibration signal and the estimation accuracy of the instantaneous fault frequency.

The arrangement of the remaining chapters is as follows: the second chapter analyzes the related work of the SST and STFRFT and discusses the existing problems. The third chapter analyzes the principles and errors of the SST. The fourth chapter proposes the FRSST algorithm and introduces the theoretical derivation and implementation steps in detail. The fifth chapter verifies the effectiveness of the method using the simulation signals and actual data from a rolling bearing. Finally, the sixth chapter summarizes the full text.

II. RELATED WORK
A rolling bearing fault signal with variable speed is nonlinear and nonstationary, rendering traditional signal processing methods ineffective [31]. The SST can concentrate the time-frequency energy of a fault signal to the real IF and improve the energy concentration of the time-frequency distribution, but the SST has two shortcomings which have been described in Section I.

A. RELATED RESEARCH OF THE SST
Based on the above shortcomings of the SST, some improved SST algorithms have appeared in recent years. In reference [32], the SST method based on variational mode decomposition (VMD) is proposed. The introduction of VMD enhances the noise robustness of the SST. In reference [33], a multiple gradually reduced synchrosqueezing transformation method is proposed that not only ensures the signal reconstruction but also improves the time-frequency concentration of the SST. In reference [34], a horizontal–vertical synchrosqueezing transformation (HV-SST) method is proposed to increase the time-frequency resolution and noise immunity by exploring the data correlation between the horizontal channel and the vertical channel. The iterative generalized SST method [17] mainly demodulates the time-frequency distribution of the nonfixed frequency signal into a straight line parallel to the time axis to improve the

instantaneous characteristic frequency extraction accuracy of the nonpure harmonic signal. However, these methods do not overcome the limitations of the SST method on the multi-component signal. The general parameterized SST [35], [36] introduces the kernel function parameters into the SST. This algorithm can not only extract the instantaneous character-istic frequency of the nonfixed frequency signal but also improve the accuracy of the instantaneous characteristic fre-quency of each component in the multicomponent signal. However, the accuracy of the method is highly dependent on the instantaneous frequency ridge extraction algorithm, and it is not suitable for a multicomponent signal with a cross instantaneous frequency. The time-reassigned syn-chrosqueezing transformation (TSST) [37] makes the time-frequency distribution coefficient redistributed in the time direction instead of in the frequency direction as in the SST. Although this transformation is more suitable for the instantaneous frequency extraction of the linear frequency modulation (LFM) signal, the calculation efficiency is low and the time-frequency resolution is not high. To improve the calculation efficiency of the TSST, an improved TSST algo-rithm is proposed in reference [38] to improve the timeliness. However, the time-frequency resolution is not improved.

In practical engineering applications, the weak fault sig-nal of a rolling bearing is more easily detected under the conditions of fluctuating speeds, while the vibration signal presents strong noise as well as nonpure harmonic and mul-ticomponent characteristics. To improve the accuracy of the IF estimation and noise robustness, we propose the FRSST algorithm.

B. RELATED RESEARCH OF THE STFRFT

The STFRFT is an important tool for LFM signal pro-cessing. It has an adaptive time-frequency-scale-frequency modulation-rate-conversion window that can reflect any local details of the signal. The STFRFT algorithm is widely used in the IF extraction of a rolling bearing [39]–[41] and some fractional models [42]–[44]. In reference [45], considering the characteristics of a rolling bearing signal, the fractional Fourier transform (FRFT) is introduced into VMD to real-ize the adaptive decomposition of VMD and improve the noise robustness of the algorithm. In [46], ensemble empirical mode decomposition based on a fractional Fourier transform was proposed to detect and estimate the parameters of multi-component chirp signals, but with the limitations of ensemble empirical mode decomposition, the modal aliasing problem is not solved well. In [47], the combination of empirical mode decomposition and a fractional Fourier transform was used to suppress high-power interference in the tracking radar signal, and some results have been achieved. However, when the interference frequency is high, the filtering effect is not obvious. In contrast to the FRFT, the STFRFT has strong time-frequency resolution and noise robustness that solve the problem that fault signals and power frequency signals are difficult to separate and extract. The STFRFT can be success-fully applied to the diagnosis of faults in asynchronous motor

rotors, as it effectively identifies the characteristic frequency and reflects the trend of the fault characteristic frequency. Therefore, according to the advantages of the STFRFT algo-rithm, the STFRFT is applied to the SST algorithm to extract the IF of a rolling bearing.

In conclusion, the FRSST method solves the problems of low accuracy of the instantaneous frequency estimation and poor noise immunity of the SST at variable speeds. First, the time-frequency distribution of each component is calculated based on the STFRFT algorithm to improve the noise robustness of the algorithm. Second, according to the SST algorithm, the time-frequency energy distribution is compressed to the real IF to improve the time-frequency concentration of the algorithm. Finally, the instantaneous fault frequency of a rolling bearing is estimated by improv-ing the peak search algorithm and the estimation error is calculated.

III. THE PRINCIPLE AND ERROR ANALYSIS OF THE SST
A. THE SST PRINCIPLE

The SST is used to compress the diffused time-frequency energy to the real instantaneous frequency, which not only improves the energy concentration of the time-frequency dis-tribution but also retains the characteristics of a signal recon-struction. The derivation process of the SST is as follows.

The definition expression of the STFT for $x(t)$ is

$$X(t, \omega) = \int_{-\infty}^{+\infty} g(u - t) \cdot x(u) \cdot e^{-j\omega u} du \qquad (1)$$

where $g(u)$ is a window function. According to Parseval's theorem, Equation (1) can be rewritten as follows:

$$\begin{aligned} X(t, \omega) &= \int_{-\infty}^{+\infty} x(u) \left(g(u - t) e^{j\omega u} \right)^* du \\ &= \int_{-\infty}^{+\infty} x(u) \cdot (g_\omega(u))^* du \\ &= \frac{1}{2\pi} \int_{-\infty}^{+\infty} \hat{x}(\xi) \cdot \left(\hat{g}_\omega(\xi) \right)^* d\xi \end{aligned} \qquad (2)$$

where $g_\omega(u) = g(u - t) \cdot e^{j\omega u}$, ()* is the symbol of a complex conjugate operation, $\hat{x}(\xi)$ is the Fourier transform of $x(u)$ and $\hat{g}_\omega(\xi)$ is the Fourier transform of $g_\omega(u)$. The expression of $\hat{g}_\omega(\xi)$ is as follows:

$$\hat{g}_\omega(\xi) = \int_{-\infty}^{+\infty} g(u - t) \cdot e^{j\omega u} \cdot e^{-j\xi u} du. \qquad (3)$$

Let $u - t = t'$. Then,

$$\begin{aligned} \hat{g}_\omega(\xi) &= \int_{-\infty}^{+\infty} g(t') \cdot e^{j\omega(t + t')} \cdot e^{-j\xi(t + t')} dt' \\ &= e^{jt(\omega - \xi)} \cdot \int_{-\infty}^{+\infty} g(t') \cdot e^{jt'(\omega - \xi)} dt' \\ &= e^{jt(\omega - \xi)} \cdot \hat{g}(\omega - \xi) \end{aligned} \qquad (4)$$

where $\hat{g}(\omega - \xi)$ is the Fourier transform of $g(\omega - \xi)$.

Substituting (4) into (2) yields

$$
\begin{aligned}
X(t, \omega) &= \frac{1}{2\pi} \int_{-\infty}^{+\infty} \hat{x}(\xi) \cdot \left(e^{jt(\omega-\xi)} \cdot \hat{g}(\omega-\xi) \right)^* d\xi \\
&= \frac{1}{2\pi} \int_{-\infty}^{+\infty} \hat{x}(\xi) \cdot e^{-j\omega t + j\xi t} \cdot \hat{g}(\omega-\xi) d\xi \\
&= e^{-j\omega t} \cdot \frac{1}{2\pi} \cdot \int_{-\infty}^{+\infty} \hat{x}(\xi) \cdot \hat{g}(\omega-\xi) \cdot e^{j\xi t} d\xi.
\end{aligned} \quad (5)
$$

The standard STFT is multiplied by the phase shift operator $e^{j\omega t}$. The resulting improved STFT is as follows:

$$
X_e(t, \omega) = \int_{-\infty}^{+\infty} x(u) \cdot g(u-t) \cdot e^{-j\omega(u-t)} du. \quad (6)
$$

The improved STFT of (6) can be rewritten into an expression corresponding to (5), as follows:

$$
X_e(t, \omega) = \frac{1}{2\pi} \cdot \int_{-\infty}^{+\infty} \hat{x}(\xi) \cdot \hat{g}(\omega-\xi) \cdot e^{j\xi t} d\xi. \quad (7)
$$

Herein, we employ the model of a purely harmonic signal (the frequency is f_0) with an invariant amplitude (A) as

$$
X(t) = A \cdot e^{jf_0 t}. \quad (8)
$$

Due to the Fourier transform of $X(t)$,

$$
\hat{X}(\xi) = 2\pi A \cdot \delta(\xi - 2\pi f_0). \quad (9)
$$

By substituting (9) into (7), we can obtain the STFT of $X(t)$:

$$
X_e(t, \omega) = A \cdot \hat{g}(\omega - 2\pi f_0) \cdot e^{j2\pi f_0 t}. \quad (10)
$$

The SST is designed to improve the energy concentration by a squeezing procedure. To obtain the instantaneous frequency of the STFT result (10), it is suggested to calculate the derivative of $X(t)$ with respect to time as

$$
\begin{aligned}
\partial_t X_e(t, \omega) &= \partial_t \left(A \cdot \hat{g}(\omega - 2\pi f_0) \cdot e^{j2\pi f_0 t} \right) \\
&= A \cdot \hat{g}(\omega - 2\pi f_0) \cdot e^{j2\pi f_0 t} \cdot j \cdot 2\pi f_0 \\
&= X_e(t, \omega) \cdot j \cdot 2\pi f_0.
\end{aligned} \quad (11)
$$

According to (10) and (11), for any (t, ω) and for $X_e \neq 0$, a 2-D instantaneous frequency $f_0(t, \omega)$ for the STFT of $X(t)$ can be obtained by

$$
f_0(t, \omega) = -j \cdot \frac{\partial_t X_e(t, \omega)}{X_e(t, \omega)}. \quad (12)
$$

In mathematics, the synchrosqueezing operator is written as $\int_{-\infty}^{+\infty} \delta(\eta - f_0(t, \omega)) d\omega$. Then, the SST is formulated as

$$
T_s(t, \eta) = \int_{-\infty}^{+\infty} X_e(t, \omega) \cdot \delta(\eta - f_0(t, \omega)) d\omega. \quad (13)
$$

The SST is the second rearrangement of the time-frequency energy of the STFT, and it can improve the energy concentration of the time-frequency distribution. Moreover, Equation (13) is integrated into the frequency domain, and the reconstructed signal of $X(t)$ can be obtained by

$$
X(t) = \frac{1}{2\pi g(0)} \cdot \int_{\{\omega, |\omega-\phi_k|<ds\}} T_x(t, \omega) d\omega \quad (14)
$$

where ϕ_k is the estimated instantaneous frequency curve and d_s is the integral interval.

B. THE ERROR ANALYSIS OF THE SST

According to (13), the result of the SST algorithm is directly affected by the estimation accuracy of the instantaneous frequency $f_0(t, w)$. According to the analysis of the SST, the instantaneous frequency of the purely harmonic signal can be estimated by (12). However, there are some errors for the LFM signal based on the SST. In this paper, the LFM signal $x(t) = \exp\left(j2\pi \left(f_0 t + \frac{1}{2}\mu t^2 \right) \right)$ and the Gaussian window function $g(t) = \exp(-\frac{t^2}{2\sigma^2})$ (σ is the standard deviation of the Gaussian window function and $\sigma \neq 0$) are taken as examples to illustrate the error of the SST algorithm. The STFT of the LFM signal is as follows:

$$
\begin{aligned}
&STFT \\
&= \int_{-\infty}^{+\infty} \exp\left(j2\pi(f_0(\tau+t) + \frac{1}{2}\mu(\tau+t)^2 - \frac{\tau^2}{2\sigma^2} - j2\pi f\tau \right) d\tau \\
&= \exp\left(j2\pi(f_0 t + \frac{1}{2}\mu t^2) \right) \int_{-\infty}^{+\infty} \exp\left(-\left(b_1\tau + a_1\tau^2 \right) \right) d\tau
\end{aligned} \quad (15)
$$

where $b_1 = -(j2\pi f_0 + j2\pi \mu t - j2\pi f)$ and $a_1 = -(j\pi\mu - \frac{1}{2\sigma^2})$. According to the integral formula

$$
\int_{-\infty}^{+\infty} e^{-(a\tau^2 + b\tau)} d\tau = \sqrt{\frac{\pi}{a}} e^{b^2/4a}. \quad (16)
$$

Equation (15) can be simplified as

$$
STFT = \sqrt{\frac{\pi}{a_1}} \exp(j2\pi(f_0 t + \frac{1}{2}\mu t^2) + b_1^2/4a_1). \quad (17)
$$

Hence,

$$
\begin{aligned}
\partial_t STFT(t, w) &= STFT \cdot j \cdot 2\pi \\
&\cdot \left((f_0 + \mu t) + \frac{j\mu(2\pi f_0 + 2\pi \mu t - 2\pi f)}{j\pi\mu - \frac{1}{2\sigma^2}} \right)
\end{aligned} \quad (18)
$$

and

$$
-j\frac{\partial_t STFTe_x}{2\pi STFTe_x} = f_0(t, w) + \frac{j\mu(2\pi f_0 + 2\pi \mu t - 2\pi f)}{j\pi\mu - \frac{1}{2\sigma^2}} \quad (19)
$$

where $f_0(t, w) = f_0 + \mu t$. If the true instantaneous frequency was estimated by (12), the error, which is $\frac{j\mu(2\pi f_0 + 2\pi \mu t - 2\pi f)}{j\pi\mu - \frac{1}{2\sigma^2}}$, would be introduced. However, the error is related to the frequency modulation rate and cannot be estimated. Therefore, the SST of the LFM signal calculated by (13) is no longer accurate. To improve the estimation accuracy of the instantaneous frequency, the SST algorithm based on the STFRST is proposed. In the following, the derivation process and calculation results of the FRSST are given.

IV. INSTANTANEOUS FREQUENCY ESTIMATION BASED ON THE FRSST

A. THE FRSST PRINCIPLE

1) THE FRFT PRINCIPLE

The FRFT is a generalized form of the traditional Fourier transform. There is a signal $f(t)$ in time-frequency domain

and the angle between its axis and time axis is β. The signal is rotated around the origin in time-frequency plane by FRFT and the rotation angle is α. When α is orthogonal to β, the energy of the signal is the most concentrated in the fractional domain as shown in the Fig. 1, where (t, w) is time-frequency plane and (u, v) is the fractional domain plane. So in the case of multicomponent, the signal is separated, and the signal is extracted by inverse fractional Fourier transform.
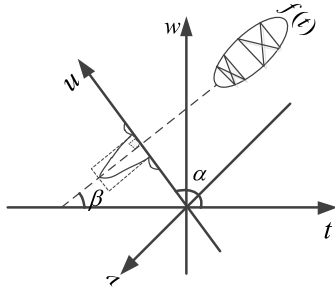

FIGURE 1. The FRFT of the signal.

The Definitions of FRFT is as follows:

$$X_\alpha(u) = FRFT_\alpha[x(t)] = \int_{-\infty}^{\infty} x(t)K_\alpha(t, u)dt \quad (20)$$

where K_α is the kernel function of the FRFT. K_α is calculated by

$$K_\alpha(t, u) = \begin{cases} A_a \exp\left[j\pi((t^2 + u^2)\cot\alpha - 2ut\csc\alpha)\right], \\ \qquad\qquad \alpha \neq n\pi \\ \delta(t - u), \quad \alpha = 2n\pi \\ \delta(t + u), \quad \alpha = (2n \pm 1)\pi \end{cases} \quad (21)$$

where $\alpha = p\pi/2$, p is the order of the FRFT and $A_a = \sqrt{1 - j\cot\alpha}$. The inverse fractional Fourier transform is the fractional Fourier transform with angle $-\alpha = -p\pi/2$, namely,

$$x(t) = \int_{-\infty}^{+\infty} X_\alpha(u)K_{-\alpha}(t, u)du. \quad (22)$$

Firstly, when FRFT is applied to fault signals of rolling bearings, the effective signal energy is concentrated in a narrow band with a certain frequency as the center, and the noise signal does not show the characteristics of energy accumulation. Therefore, the FRFT can better separate the noise part of the fault signal and improve the anti-noise ability of the algorithm. Secondly, there are many frequency components in the fault signal, and they are cross-interference, which will greatly increase the difficulty of frequency estimation. But each frequency component has different energy aggregation center frequencies in the fractional domain. Therefore, the FRFT can effectively suppress cross-interference and improve the estimation accuracy of the frequencies of each component. Therefore, the FRFT instead of Fourier transform is applied to the SST algorithm.

2) THE STFRFT PRINCIPLE

According to the characteristics of the FRFT, the STFRFT with order α of a function $x(t)$ is defined as the convolution of the FRFT and a window function and is calculated by

$$STFRFT_\alpha(t, u) = \int_{-\infty}^{+\infty} x(t + \tau)g^*(\tau)K_\alpha(\tau, u)d\tau. \quad (23)$$

3) THE DETECTION AND PARAMETERS ESTIMATION OF AN LFM SIGNAL

As the FRFT is a 1-D linear change, it is unaffected by cross terms. The FRFT can not only detect and estimate the parameters of an LFM signal reliably but also reduce the complexity of the processing. The specific steps are as follows. The LFM signal with noise can be expressed as

$$x_1(t) = s(t) + w(t) = a_0 \exp(j\varphi_0 + j2\pi f_0 t + \pi\mu_0 t^2) + w(t) \quad (24)$$

where a_0, φ_0, f_0 and ζ_0 are unknown parameters and $w(t)$ is Gaussian white noise. Then, the process of optimal order selection and parameter estimation for (24) can be described as

$$\{\hat\alpha_0, \hat u_0\} = \arg \max_{\alpha, u} |X_\alpha(u)|^2 \quad (25)$$

and

$$\begin{cases} \widehat\mu_0 = -\cot\hat\alpha_0 \\ \hat f_0 = \hat u_0 \csc\hat\alpha_0 \\ \hat\varphi_0 = \arg\left[\dfrac{X_{\hat\alpha_0}(\hat u_0)}{A_{\hat\alpha_0}e^{j\pi\hat u_0^2 \cot\hat\alpha_0}}\right] \\ \hat a_0 = \dfrac{|X_{\hat\alpha_0}(\hat u_0)|}{\Delta t |A_{\hat\alpha_0}|} \end{cases} \quad (26)$$

where $X_\alpha(u)$ is the FRFT of $x_1(t)$ and $\widehat\mu_0$, $\hat f_0$, $\hat\varphi_0$ and $\hat a_0$ represent the parameter estimation of the frequency modulation rate, center frequency, phase and amplitude of the LMF signal, respectively.

4) THE FRSST PRINCIPLE

In this section, the LFM signal $x(t) = \exp\left(j2\pi\left(f_0 t + \frac{1}{2}\mu t^2\right)\right)$ and the Gaussian window function $g(t) = \exp(-\frac{t^2}{2\sigma^2})$ (σ is the standard deviation of the Gaussian window function and $\sigma \neq 0$) are taken as examples to illustrate the advantages and principle of the FRSST. The FRSST algorithm has two advantages, and one is to improve the energy concentration of the time-frequency distribution. According to reference [48], the difference between the STFT and STFRFT in the time-frequency resolution of an LFM signal is mainly caused by $4\pi^2\sigma^4\mu^2$. With the increase of μ, the time-frequency concentration of the STFT decreases, while the corresponding concentration of the STFRFT is unaffected by μ. The second advantage of the FRSST algorithm is to improve the estimation accuracy of the instantaneous frequency. This second advantage is explained in detail by a theoretical derivation.

According to the analysis in Section III.B, if the true instantaneous frequency is estimated by (12), the error of $\frac{j\mu(2\pi f_0 + 2\pi\mu t - 2\pi f)}{j\pi\mu - \frac{1}{2\sigma^2}}$ would be introduced. The error that cannot be estimated is related to the frequency modulation rate μ. Therefore, the SST of the LFM signal calculated by (13) is no longer accurate. The FRSST algorithm avoids the problem and increases the estimation accuracy of the instantaneous frequency. The FRSST principle is described below. In addition, the ideal method to avoid the problem is explained below.

The STFRFT with order α of a function $x(t)$ is defined as

$$STFRFT_\alpha(t, u)$$

$$= A_\alpha \int_{-\infty}^{+\infty} \left[\begin{array}{c} \exp(j2\pi(f_0(t+\tau) + \frac{1}{2}\mu(t+\tau)^2) \cdot \exp(-\frac{\tau^2}{2\sigma^2}) \\ \cdot \exp(j\pi(\tau^2\cot\alpha + u^2\cot\alpha - 2u\tau\csc\alpha))d\tau \end{array} \right]$$

$$= A_\alpha \exp(j2\pi(f_0 t + \frac{1}{2}\mu t^2) + j\pi u^2 \cot\alpha)$$

$$\cdot \int_{-\infty}^{+\infty} \left[\begin{array}{c} \exp((j2\pi f_0 + j2\pi\mu t - j2\pi u\csc\alpha)\tau) \\ \cdot \exp((j\pi\mu + j\pi\cot\alpha - \frac{1}{2\sigma^2})\tau^2)d\tau \end{array} \right]$$

$$= A_\alpha \exp(j2\pi(f_0 t + \frac{1}{2}\mu t^2) + j\pi u^2 \cot\alpha)$$

$$\cdot \int_{-\infty}^{\infty} \exp(-(B\tau + A\tau^2))d\tau \quad (27)$$

where $B = -(j2\pi f_0 + j2\pi\mu t - j2\pi u\csc\alpha)$ and $A = -(j\pi\mu + j\pi\cot\alpha - \frac{1}{2\sigma^2})$. According to (16), Equation (27) can be rewritten as

$$STFRFT_\alpha(t, u) == A_\alpha \exp(j2\pi(f_0 t + \frac{1}{2}\mu t^2) + j\pi u^2 \cot\alpha)$$

$$\cdot \sqrt{\frac{\pi}{A}} \cdot \exp(B^2/4A)$$

$$= \sqrt{\frac{\pi}{A}} A_\alpha \exp(j2\pi(f_0 t + \frac{1}{2}\mu t^2)$$

$$+ j\pi u^2 \cot\alpha + B^2/4A) \quad (28)$$

According to (28), the time-frequency energy distribution of $x(t)$ based on the STFRFT appears energy diffusion with $w = f_0 + \mu t$ as the center. To reduce the energy diffusion caused by the STFRFT, the SST is designed to compress the energy to the instantaneous frequency. The derivative of $STFRFT_\alpha(t, u)$ with respect to time is

$$\partial_t STFRFT_\alpha(t, u)$$

$$= \partial_t \left(\sqrt{\frac{\pi}{A}} A_\alpha \exp(j2\pi(f_0 t + \frac{1}{2}\mu t^2) + j\pi u^2\cot\alpha + B^2/4A) \right)$$

$$= STFRFT_\alpha(t, u) \cdot (j2\pi(f_0 + \mu t) + \frac{B}{2A}\frac{\partial B}{\partial t})$$

$$= STFRFT_\alpha(t, u) \cdot (j2\pi(f_0 + \mu t) + 2\pi\mu$$

$$\cdot \frac{2\pi(u\csc\alpha - f_0) - \pi\mu t}{\frac{1}{\sigma^2} - j2\pi(\mu + \cot\alpha)}) \quad (29)$$

According to (26), when α is the optimal order, $f_0 = u\csc\alpha$ and $\mu = -\cot\alpha$. Therefore, Equation (29) is simplified as

$$\partial_t STFRFT_\alpha(t, u)$$

$$= STFRFT_\alpha(t, u) \cdot (j2\pi(f_0 + \mu t) - 2\pi^2\sigma^2(\cot^2\alpha)t). \quad (30)$$

According the properties of FRFT, $u = w \cdot \cos\alpha$. By substituting this equation into (30), for any (t, w), a 2-D instantaneous frequency for the STFRFT can be obtained by

$$f(t, w) = f_0 + \mu t$$

$$= -j\frac{\frac{\partial_t STFRFT_\alpha(t, w)}{STFRFT_\alpha(t, w)} + 2\pi^2\sigma^2(\cot^2\alpha)t}{2\pi}. \quad (31)$$

From the above analysis, it can be seen that the STFRFT can improve the instantaneous frequency estimation accuracy of an LFM signal compared with the STFT algorithm.

The FRSST is a synchrosqueezing transformation based on the STFRFT. The synchrosqueezing operator is written as $\int_{-\infty}^{+\infty} \delta(\eta - f(t, \omega))d\omega$, and the FRSST is formulated as

$$FRSST_x(t, \eta) = \int_{-\infty}^{\infty} STFRFT_\alpha(t, w)\delta(\eta - f(t, w))d\omega. \quad (32)$$

The SST that is the second rearrangement of the time-frequency energy of the STFRFT can improve the energy clustering of the time-frequency distribution. Moreover, Equation (32) is integrated into the frequency domain, and the reconstructed signal of $x(t)$ can be obtained by

$$x(t) = (2\pi g(0))^{-1} \cdot \int_{\{w, |w-\phi_k < ds\}|} FRSST_x(t, w)dw \quad (33)$$

where ϕ_k is the estimated instantaneous frequency curve and d_s is the integral interval.

B. INSTANTANEOUS FREQUENCY RIDGE EXTRACTION

The vibration signal of a rolling bearing not only has the characteristics of emphasizing frequency but also is easily affected by noise. Therefore, in its time-frequency energy distribution, there may be multiple peaks at the same time, and the peak component caused by noise is often higher than the corresponding peak of the effective signal. To extract the instantaneous frequency ridge more accurately, an improved peak search algorithm is proposed [49].

(1) The coordinates (n_0, k_0) and (n_1, k_1) of two adjacent peaks at the starting point are obtained based on the basic peak search method, and the first derivative at the two points is calculated by $d_0 = d_1 = \frac{k_1 - k_0}{n_1 - n_0}$.

(2) The frequency search range is set as $(k_1 - p, k_1 + p)$ at time n_2, where p should be sufficiently large to ensure that the instantaneous frequency is within the search range. Moreover, all of the searched peaks in the range are inserted into array B according to the magnitude order of the amplitude.

(3) The maximum value $B(1)$ of B is taken, and d_2 and ε_2 are calculated by $d_2 = \frac{B(1) - k_1}{n_2 - n_1}$ and $\varepsilon_2 = |d_2 - d_1|$, respectively.

(4) After setting the threshold value s based on reference [49], ε_2 and s are compared. If s is larger, $B(1)$ is the frequency at time n_2. Otherwise, the next point of array B is taken as the frequency, and steps (3) and (4) are repeated until $B(i)$ is smaller than s. Thus, $B(i)$ is the frequency at time n_2 and the point (n_2, k_2) is derived.

(5) Steps (1), (2), (3) and (4) are repeated with (n_2, k_2) instead of (n_0, k_0), and in this way the frequency at each time can be obtained.

The improved peak search method can effectively avoid the false peak values extracted by the traditional peak search method.

C. INSTANTANEOUS FREQUENCY ESTIMATION OF A MULTICOMPONENT SIGNAL BASED ON THE ITERATIVE FRSST

There may be different strength and frequency vibration signals in the rolling bearing at the same time. Based on the iterative FRSST, the instantaneous frequency of each component vibration signal is extracted in turn. The specific steps are as follows:

(1) In the (α, u) plane, the position of the strongest signal component $(\widehat{\alpha}_{01}, \widehat{u}_{01})$ and the corresponding parameter estimation $\left\{ \widehat{a}_{01}, \widehat{\varphi}_{01}, \widehat{f}_{01}, \widehat{\mu}_{01} \right\}$ are obtained according to (25) and (26) by a 2-D search.

(2) The STFRFT with order $\widehat{\alpha}_{01}$ of function $x(t) = s(t) + w(t)$ is defined as (34), where $s(t)$ is the multicomponent signal and $w(t)$ is Gaussian white noise.

$$X_{STFRFT}^{\widehat{\alpha}_{01}}(u) = S_{STFRFT}^{\widehat{\alpha}_{01}}(u) + W_{STFRFT}^{\widehat{\alpha}_{01}}(u) \qquad (34)$$

where $S_{STFRFT}^{\widehat{\alpha}_{01}}(u)$ and $W_{STFRFT}^{\widehat{\alpha}_{01}}(u)$ are the STFRTs of the multicomponent signal and the noise signal, respectively. At this time, most of the energy of the first component is concentrated in a narrow band centered on the real instantaneous frequency of the component, while the noise and other signals do not show obvious energy accumulation.

(3) The time-frequency energy of the FRSST for the signal is obtained by (32), and the instantaneous frequency ridge is obtained by the improved peak search in Section IV.B.

(4) The time domain signal corresponding to the frequency component is recovered by (33).

(5) By repeating the above steps for the remaining components $x'(t) = x(t) - \widehat{s}_1(t)$ until the amplitude of the residual signal is lower than a predetermined threshold value, the instantaneous frequency ridge and time domain signal estimation for each component of the multicomponent signal can be obtained.

D. EVALUATION INDEXES

In this paper, a time-frequency energy concentration index and two error analysis indexes are introduced to represent the effectiveness of the FRSST, namely, the Renyi entropy, instantaneous frequency extraction error and the improvement of the signal-to-noise ratio (SNR), respectively.

(1) Renyi entropy

The Renyi entropy can be used to quantitatively analyze the energy concentration of time-frequency analysis methods, and it is an important index to evaluate the time-frequency resolution. The Renyi entropy is defined as

$$R_\beta(TF(t,f)) = \frac{1}{1-\beta} \log_2 \int_{-\infty}^{\infty} \int_{-\infty}^{\infty} TF^\beta(t,f) dt df \qquad (35)$$

where $TF(t,f)$ is the time-frequency distribution and $\beta = 3$. A smaller Renyi entropy implies a better time-frequency energy aggregation and a higher time-frequency resolution.

(2) Estimation error of the instantaneous frequency

The real instantaneous frequency is $f(t)$, and the estimate is $\widehat{f}(t)$. The mean absolute error between them is used to represent the estimation error of the instantaneous frequency, and its expression is as follows:

$$\sigma = \frac{1}{m} \sum_{i=1}^{m} \left| \widehat{f}(i) - f(i) \right| \qquad (36)$$

where m is the number of samplings.

(3) The improvement of the SNR

To analyze the anti-noise ability of the algorithm intuitively, the SNR is introduced; it is the ratio of the signal energy to the noise energy. The input signal is set as $v(t) = s(t) + w(t)$, where $s(t)$ is the useful signal and $w(t)$ is the noise. Then, the input SNR (SNR_{in}) is formulated as

$$SNR_{in} = \frac{\sum_{i=1}^{m} s^2(i)}{\sum_{i=1}^{m} w^2(i)}. \qquad (37)$$

The output SNR is the ratio of the energy of the useful signal to the energy of the residual noise in the noise reduced signal $\widehat{v}(t)$. The output SNR (SNR_{out}) is formulated as

$$SNR_{out} = \frac{\sum_{i=1}^{m} s^2(i)}{\sum_{i=1}^{m} [\widehat{v}(i) - s(i)]^2}. \qquad (38)$$

The improvement of the SNR (SNR_{dif}) is the difference between SNR_{out} and SNR_{in}, which is calculated by

$$SNR_{dif} = SNR_{out} - SNR_{in}. \qquad (39)$$

V. EXPERIMENT ANALYSIS

In this paper, the FRSST algorithm is compared with the SST, the VMD-SST and PSST based on the simulated signal and a rolling bearing's actual data. In the comparison part of the simulated signal, by constructing different simulation signals, we verified that the FRSST algorithm has a high time-frequency concentration, is non-fragile to the frequency modulation rate, has noise robustness and features nonsensitivity to cross-frequency signals. For the actual signal, the outer ring fault signal of a rolling bearing was obtained from the QPZZ-II fault simulation platform for

comparison and verification. The energy concentration of the time-frequency distribution of the rolling bearing vibration signal and the estimation accuracy of the instantaneous fault frequency are compared and verified.

A. SIMULATION SIGNAL ANALYSIS
1) THE HIGH TIME-FREQUENCY CONCENTRATION OF THE FRSST
To verify the time-frequency concentration of the FRSST, the nonlinear frequency modulation signal is used in the simulation experiment, and it is modeled as

$$S(t) = \exp(j2\pi(40t - 50t^2 + 70t^3)). \quad (40)$$

The sampling frequency f_s is 1024 Hz that means the proposed approach collects 1024 samples/second, and the sampling time is one second. Based on the SST and FRSST methods, the time-frequency distribution of the signal is shown in Fig. 2.
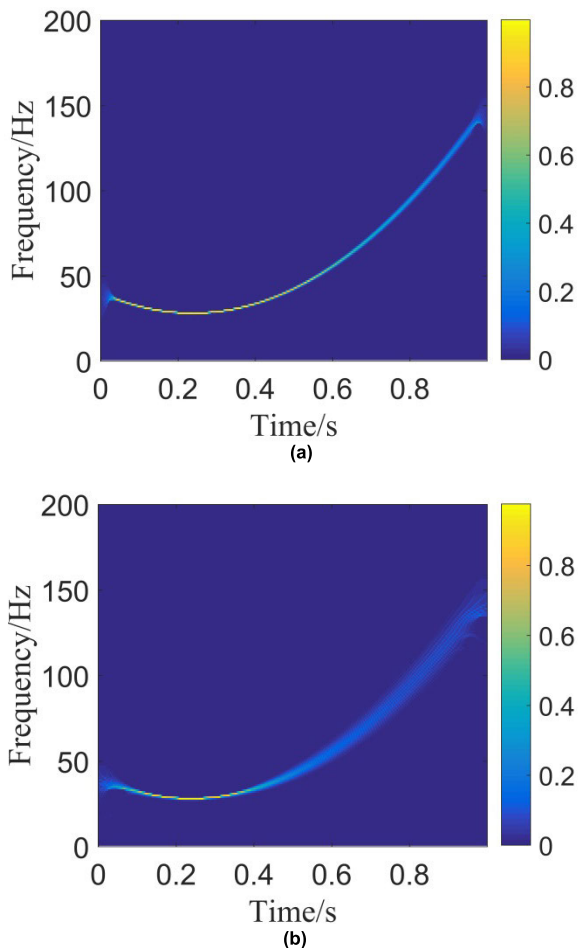
FIGURE 2. The time-frequency distribution of the signal: (a) The time-frequency distribution based on the FRSST; (b) The time-frequency distribution based on the SST.

As shown in Fig. 2, when the frequency modulation rate is low, the SST and FRSST algorithms have similar time-frequency concentrations. However, with the increase of

the frequency modulation rate, the FRSST can still ensure good time-frequency concentration, while the time-frequency energy of the SST is dispersed. Therefore, the time-frequency concentration of the SST decreases in the period with a large frequency change rate, while the frequency change rate has no effect on the FRSST. According to (35), the Renyi entropies of the two algorithms are shown in Table 1, and it can be seen that the FRSST has better time-frequency concentration than the SST.

TABLE 1. The Renyi entropies of the SST and FRSST.

Algorithm	Renyi entropy
SST	11.61
FRSST	10.70

2) NON-FRAGILE OF THE FRSST TO THE FREQUENCY MODULATION RATE
A multicomponent LFM simulated signal is constructed as follows:

$$S_1(t) = s_1(t) + s_2(t) + s_3(t) + s_4(t) \quad (41)$$

where the math model of each component is written as

$$s_1(t) = 1.5\exp(j0 + j2\pi(50t + 0t^2)) \quad (42)$$
$$s_2(t) = 2\exp(j0 + j2\pi(120t + 5t^2)) \quad (43)$$
$$s_3(t) = 3\exp(j0 + j2\pi(190t + 15t^2)) \quad (44)$$
$$s_4(t) = 3.5\exp(j0 + j2\pi(260t + 35t^2)) \quad (45)$$

The sampling frequency f_s is 1000 Hz that means the proposed approach collects 1000 samples/second, and the sampling time is one second. The time domain waveform and the frequency spectrum of $S_1(t)$ are shown in Fig. 3.

Since the simulation signal is nonstationary, the frequency component of the signal can no longer be identified by the fast Fourier transform (FFT), as shown in Fig. 3 (b). The proposed FRSST method is used to process the multicomponent signal. According to the calculation steps shown in Section IV.C, a time-frequency representation of each component signal is obtained by the FRSST and a similar representation of the simulation signal $S_1(t)$ can be obtained by adding those representations, which is shown in Fig. 4.

To illustrate the effectiveness of the FRSST, the instantaneous frequency estimation of each component and the estimation error of the instantaneous frequency of the FRSST algorithm is compared with the corresponding figures for the VMD-SST and PSST algorithms. The instantaneous frequency trajectories shown in Fig. 5 are extracted by the improved peak search algorithm in Section IV.B. As shown in Fig. 5, with the increase of the frequency modulation rate, the estimation errors of the instantaneous frequency by the VMD-SST and PSST algorithm grow, while the estimation error of the FRSST algorithm is less affected by the frequency modulation rate. To further illustrate the non-fragile of the FRSST algorithm to the frequency modulation rate,
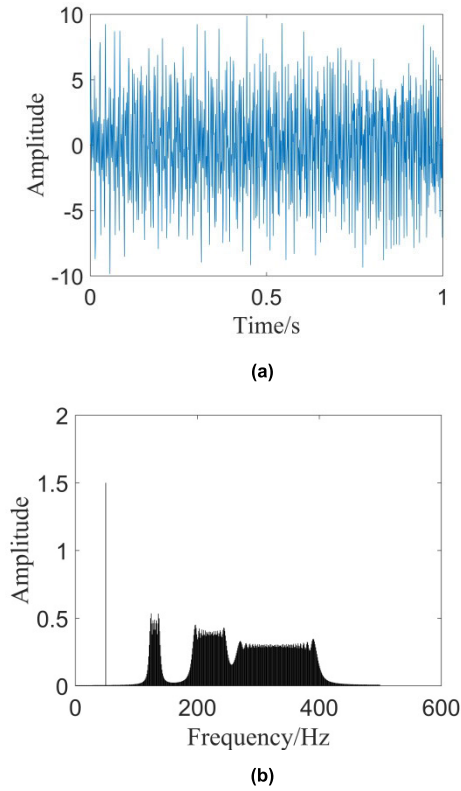
(a)

(b)

FIGURE 3. The time domain waveform and the frequency spectrum of $S_1(t)$: (a) The time domain waveform; (b) The frequency spectrum.
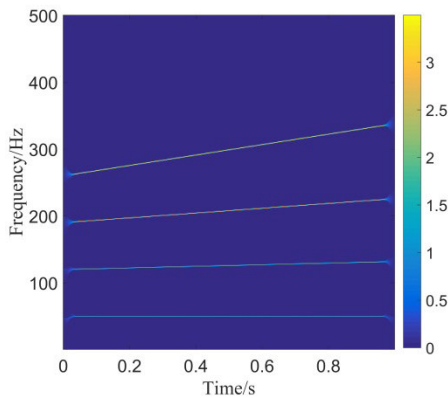

FIGURE 4. The time-frequency representation of $S_1(t)$ based on the FRSST.

the relationship between the frequency modulation rate and the estimation error of the instantaneous frequency is shown in Fig. 6 by changing the frequency modulation rate in the range of 0-100 in steps of 5. The Renyi entropy changing with the frequency modulation rate is shown in Fig. 7.

As shown in Fig. 6, with the increase of the frequency modulation rate, the estimation error of the instantaneous frequency based on the VMD-SST and PSST increases gradually, and the error variation amplitude also increases. The estimation error based on the FRSST algorithm is less than the estimation errors of the VMD-SST and PSST algorithms,
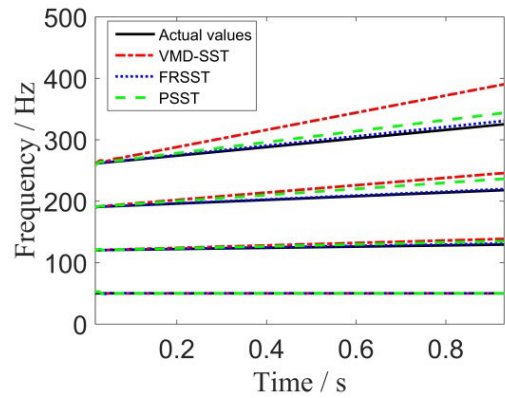

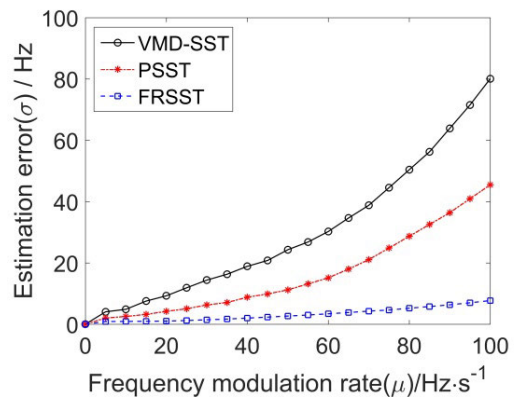**FIGURE 5.** Instantaneous frequency trajectories.

FIGURE 6. The relationship between the frequency modulation rate and the estimation error of the instantaneous frequency.

furthermore, the error variation amplitude changes little with the increase of the frequency modulation rate. Therefore, we know that the FRSST method has a strong non-fragile to the frequency modulation rate. For the VMD-SST and PSST, the derivative of the STFT with respect to time is calculated to obtain the instantaneous frequency, which will introduce the estimation error of the instantaneous frequency, and the simulation results are consistent with the result of (19). While in the FRSST, Equation (31) is used to replace the estimation of the instantaneous frequency on the STFT, and the estimation accuracy of the instantaneous frequency of each component is greatly improved. As shown in Fig. 7, the Renyi entropy of the VMD-SST and PSST increases with the increase of the frequency modulation rate, and the time-frequency concentration decreases. However, the Renyi entropy of the FRSST does not change much, and its time-frequency concentration is higher than the time-frequencies of the VMD-SST and PSST. This behavior occurs because the time-frequency concentration of the STFT decreases with the increase of the frequency modulation rate, while the corresponding concentration of the STFRFT is not affected by the frequency modulation rate. Through the comparison of the above performance indexes, it can be seen that the FRSST algorithm has a strong non-fragile to the frequency modulation rate.
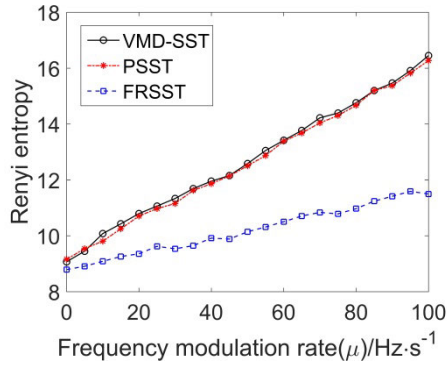
FIGURE 7. The Renyi entropy changing curve.

3) NOISE ROBUSTNESS OF THE FRSST

To verify the noise robustness of the FRSST, different SNRs are added to the signal in (41), and the signals with noise are obtained as

$$S_2(t) = S_1(t) + \eta(t) \tag{46}$$

where $S_1(t)$ is as shown in (41) and $\eta(t)$ is Gaussian white noise. $SNR_{in} = -2$ dB, which is taken as an example for experimental comparison and demonstration. Instantaneous time-frequency representation of the signal is shown in Fig. 8 when $SNR_{in} = -2$ dB. The following quantified indicators including the instantaneous frequency estimation of each component and the improvement of the SNR are considered. The advantages of the FRSST are compared with the VMD-SST and PSST. The comparison result of the instantaneous frequency trajectories is displayed in Fig. 9, which shows that the instantaneous frequency trajectories based on the VMD-SST method have the lowest accuracy and have many burrs. Compared with the VMD-SST, the accuracy of the instantaneous frequency based on the PSST is improved, but there are still many burrs. The estimation accuracy of the instantaneous frequency is higher and the instantaneous frequency trajectories are smoother based on the FRSST algorithm. To further illustrate the noise robustness of the
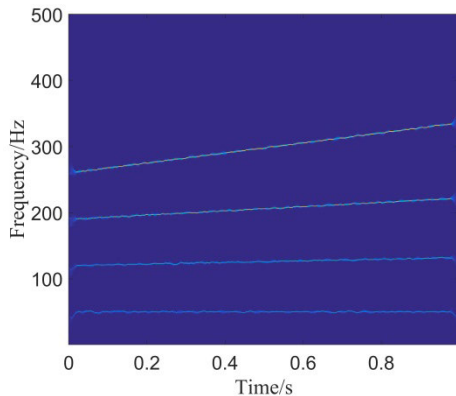

FIGURE 8. Instantaneous time-frequency representation of $S_2(t)$ based on the FRSST.
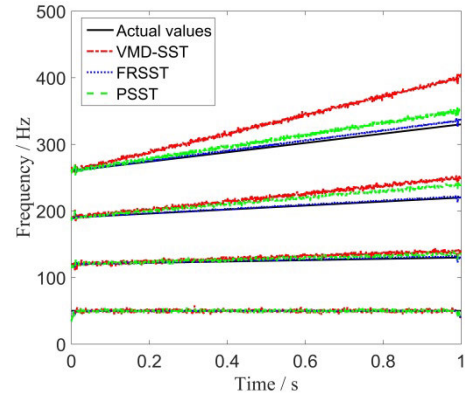
FIGURE 9. Instantaneous frequency trajectories.

FRSST method, the relationship between SNR_{in} and SNR_{dif} is shown in Fig. 10 by changing SNR_{in} in the range of [-15 15] dB in steps of 1 dB.
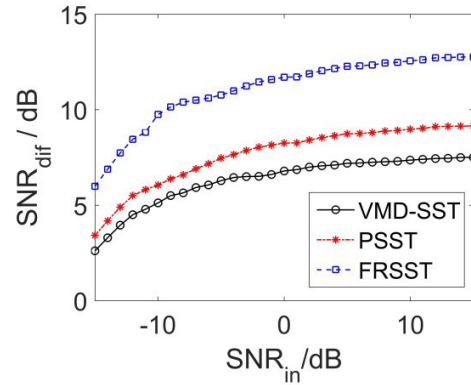

FIGURE 10. The improvement of the SNR with different SNR_{in}.

As shown in Fig. 10, with the increase of SNR_{in}, the SNR_{dif} of the FRSST is more than those of the VMD-SST and PSST, which implies that the FRSST has strong noise robustness. This finding is sensible because both the VMD-SST and the PSST are based on the STFT, which has poor noise immunity. Furthermore, the FRSST method uses the STFRFT instead of the STFT and makes full use of the noise immunity of the STFRFT. Thus, the FRSST has strong noise robustness.

4) NONSENSITIVITY OF THE FRSST TO CROSS-FREQUENCY SIGNALS

When the instantaneous frequency of the signal is crossed, there will be cross interferences in the time-frequency analysis. To verify the effectiveness of the FRSST for the cross-frequency signal, a multicomponent signal with a cross frequency is constructed as

$$S_3(t) = s_5(t) + s_6(t) \tag{47}$$

where the math model of each component is written as

$$s_5(t) = 3\exp(j0 + j2\pi(190t + 5t^2)) \tag{48}$$
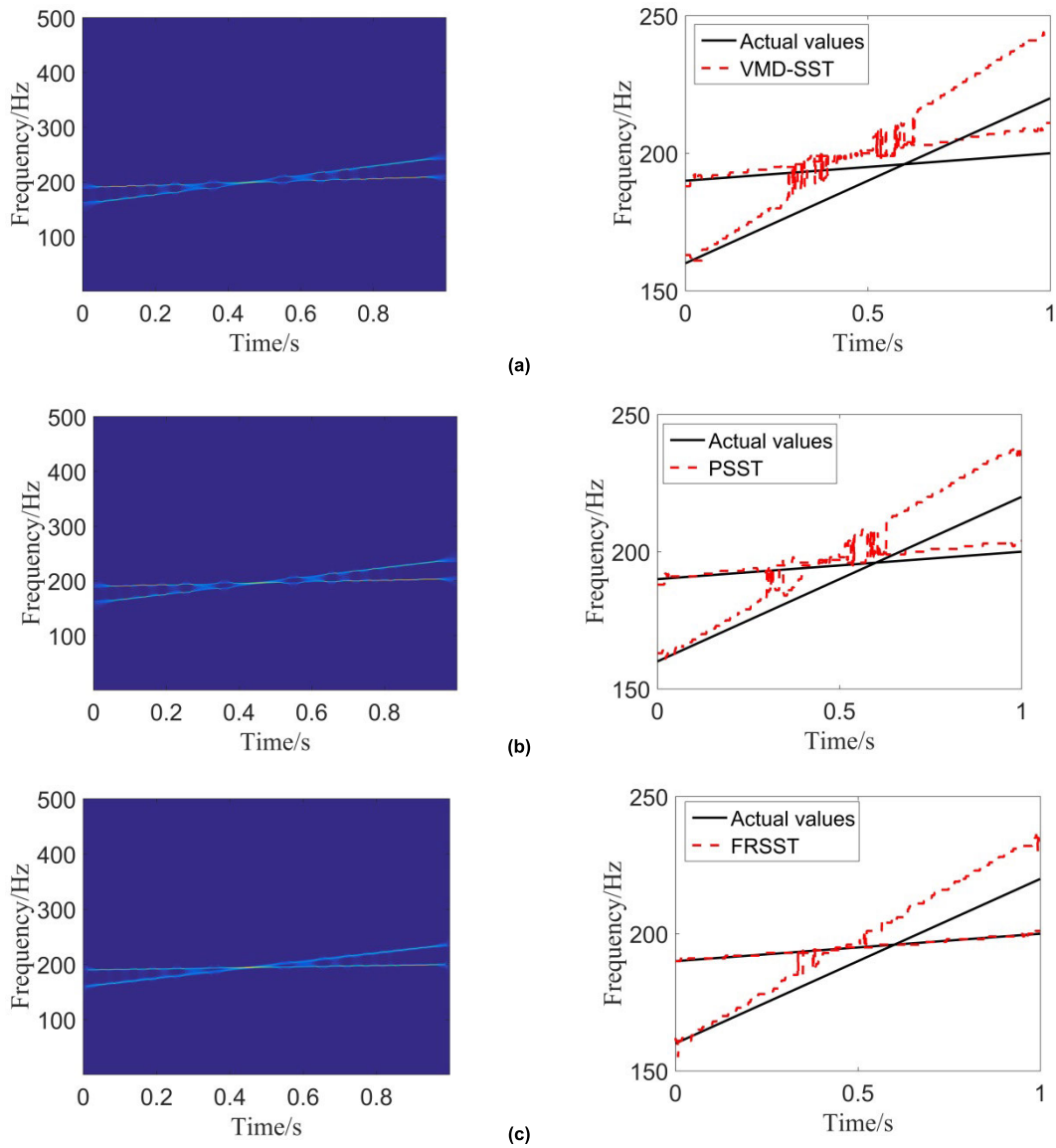$$s_6(t) = 2\exp(j0 + j2\pi(160t + 30t^2)) \tag{49}$$

FIGURE 11. Instantaneous time-frequency representation and instantaneous frequency trajectories of a cross-frequency signal: (a) Instantaneous time-frequency representation based on the VMD-SST and the instantaneous frequency trajectories; (b) Instantaneous time-frequency representation based on the PSST and instantaneous frequency trajectories; (c) Instantaneous time-frequency representation based on the FRSST and the instantaneous frequency trajectories.

The FRSST, VMD-SST and PSST algorithms are used to estimate the instantaneous frequency, and the results are shown in Fig. 11.

As shown in Figs. 11 (a) and (b), the instantaneous frequency energy of the VMD-SST and PSST at the intersection are divergent, and the instantaneous frequency is marred by confusion and ambiguity. In Fig. 11(c), the FRSST has a high time-frequency resolution, and the instantaneous frequency ridge is clear and still effective. It can be seen that the duration of the cross ambiguity based on the VMD-SST and PSST is 0.3 s, and the corresponding duration of the FRSST is less than 0.1 s on the left side of the intersection, which greatly reduces the frequency estimation error. Thus, the accuracy of the instantaneous frequency estimation of the FRSST is still

better than the corresponding accuracies of the VMD-SST and PSST for cross-frequency signals and the FRSST is still valid for such signals.

B. ACTUAL SIGNAL ANALYSIS OF A FAULT BEARING

The equipment used in this paper is the QPZZ-II fault simulation platform which is a rotating machinery vibration and fault simulation platform, as shown in Fig. 12. The components of the QPZZ-II are shown in Fig. 12(a). Fig. 12(b) is a part of the simulation platform with a fault bearing and the sensor is marked. The simulation schematic diagram is shown in Fig.12 (c). The tachometer is XB40-I type. The bearing type is NU205EM, the front end is normal bearing, and the back end is fault bearing to be tested. The acceleration
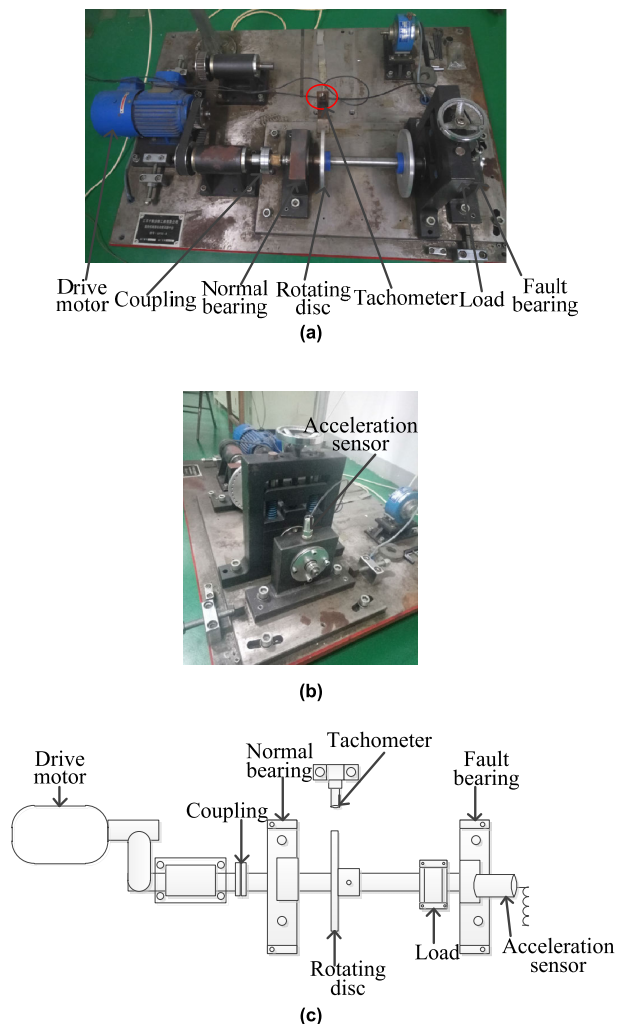
FIGURE 12. The experimental platform: (a) QPZZ-II fault simulation platform; (b) The sensor installation position; (c) The simulation schematic diagram.

sensor is CA-YD-188 type and the drive motor is YVF801-4 which is AC variable frequency motor with speed range of 75-1450rpm. The load type is CZ-0.5 which is the magnetic powder brake and it is radial force with maximum torque of 5N·m. The rotational speed of the rotating disc that is installed on the transmission shaft is measured by the tachometer, and the rotating frequency of the bearings is obtained. The vibration signal of the fault bearing is measured by the acceleration sensor to provide the experimental data of the fault bearing for the following. Moreover, the main parameters of the bearing are shown in Table 2.

TABLE 2. The main parameters of the bearing.

Diameter of pitch circle	Diameter of rolling body	Contact angle	The number of rolling bodies
38.5 mm	7.5	0°	13

When the rotational speed of a rolling bearing is constant, the high amplitude and fast attenuation impact will be produced in the vibration signal because of the collision between the fault point and its corresponding mating surface. And with the continuous operation of a rolling bearing, the impact will occur repeatedly at a fixed time interval, the repetition frequency is the fault characteristic frequency (IFF) which is the IF harmonics. When the outer ring, inner ring, rolling element or cage of rolling bearing fails, the calculation formulas of IFF [50] are as follows:

$$IFF_o = \frac{nf_r}{2}\left(1 - \frac{d}{D}\cos\varphi\right) \tag{50}$$

$$IFF_i = \frac{nf_r}{2}\left(1 + \frac{d}{D}\cos\varphi\right) \tag{51}$$

$$IFF_b = \frac{Df_r}{2d}\left[1 - \left(\frac{d}{D}\right)^2\cos^2\varphi\right] \tag{52}$$

$$IFF_c = \frac{f_r}{2}\left[1 - \frac{d}{D}\cos\varphi\right] \tag{53}$$

where IFF_o, IFF_i, IFF_b, IFF_c represent the IFF of outer ring, inner ring, rolling element and cage respectively, n is the number of rolling bodies, d is the diameter of rolling body, D is the diameter of pitch circle, φ is the contact angle and f_r is the IF.

The feasibility of the FRSST method was verified by measuring the fault signals of an outer ring rolling bearing with rising speed and complex fluctuated speed.

1) THE INSTANTANEOUS FREQUENCY ESTIMATION OF A ROLLING BEARING WITH RISING SPEED

The fault signal of the outer ring of the rolling bearing under the condition of rising speed is analyzed. During the test, the sampling frequency is 25600 Hz and the sampling time is 4 s. Only the acceleration signal collected by the vertical acceleration sensor is used for the test analysis, and its time domain, frequency domain waveform and instantaneous rotational frequency curve are shown in Figs. 13 (a), (b) and (c), respectively. According to (50), the theoretical value curve of the instantaneous fault frequency is shown in Fig. 13 (d).

If the amplitudes of the instantaneous fault frequency IFF_o and 2 and 3 times frequency are more prominent, the bearing fault can be judged [51]. The time-frequency energy distribution based on the FRSST, VMD-SST and PSST algorithms are shown in Fig. 14.

As shown in Fig. 14, 1, 2 and 3 times of the IFF can be extracted by the FRSST. The time-frequency concentrations of the FRSST, VMD-SST and PSST are analyzed by the Renyi entropy, and the results are shown in Table 3. According to the comparison in Table 3, the Renyi entropy of the FRSST is the smallest and the time-frequency concentration is the highest. The IFF trajectories shown in Fig. 15 are extracted by the improved peak search algorithm. The estimation error of the IFF based on the FRSST method is the least, and it is 2.1856 Hz less than the corresponding error
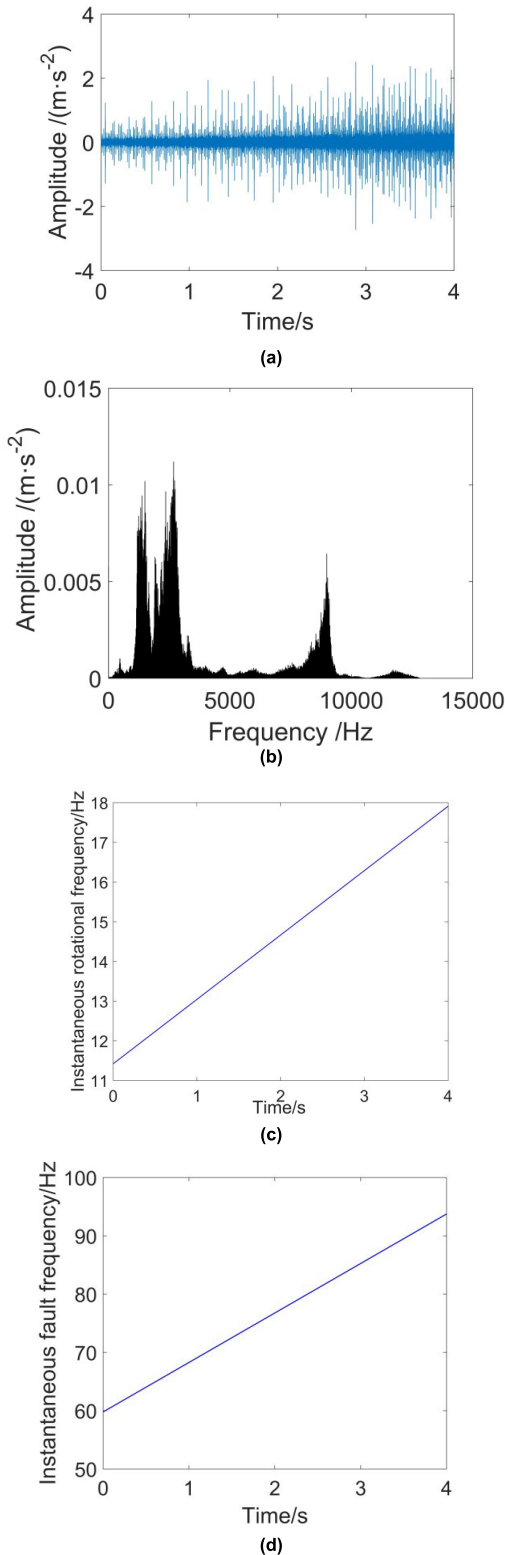
FIGURE 13. The signal preprocessing results for actual signals: (a) Time domain diagram; (b) Frequency domain waveform; (c) Instantaneous rotational frequency curve; (d) Instantaneous fault frequency curve.

FIGURE 14. Instantaneous time-frequency representations: (a) FRSST; (b) VMD-SST; (c) PSST.

TABLE 3. The Renyi entropy.

Algorithms	Renyi entropy
FRSST	16.052
VMD-SST	20.6641
PSST	19.954

of the VMD-SST and 1.1879 Hz less than the corresponding error of the PSST method.

In order to further verify the effectiveness of the FRSST algorithm, the comparison results of Renyi entropy and
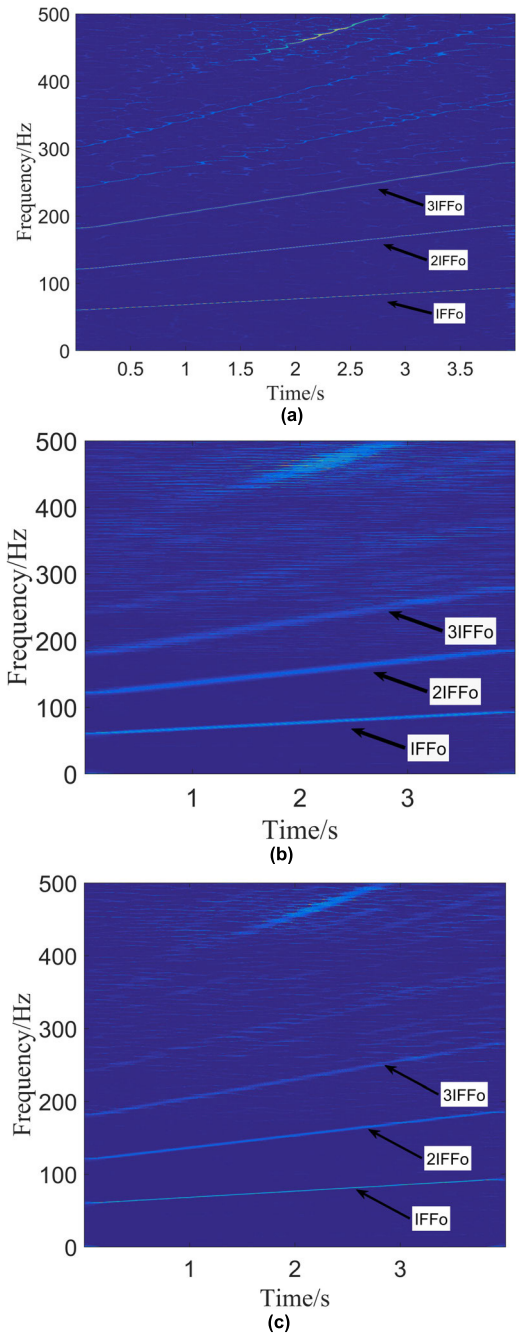
estimation error of IFF of the other three cases are obtained by changing the fault type of a rolling bearing under the same speed condition, as shown in Table 4. The estimation error of IFF based on the FRSST method is the least for the four fault
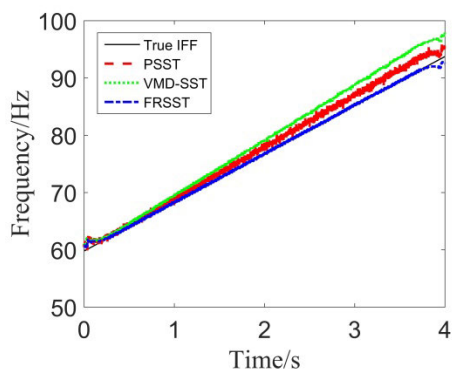
FIGURE 15. The IFF estimation for actual signals.

TABLE 4. The Renyi entropy and Estimation error of IFF under different type of faults.

Algorithm	Inner ring fault		Rolling element fault		Cage fault	
	Renyi entropy	Error of IFF (Hz)	Renyi entropy	Error of IFF (Hz)	Renyi entropy	Error of IFF (Hz)
FRSST	16.324	0.1743	17.125	0.1789	17.523	0.1792
VMD-SST	20.984	2.3840	21.048	2.4125	21.487	2.4223
FRSST	19.987	1.3548	20.154	1.3662	20.854	1.3682

types. On average, the estimation error is 2.2180 Hz less than the corresponding error of the VMD-SST and 1.1862 Hz less than the corresponding error of the PSST method.

2) THE INSTANTANEOUS FREQUENCY ESTIMATION OF A ROLLING BEARING WITH FLUCTUATED SPEED

The fault signal of the outer ring of the rolling bearing with complex fluctuated speed is analyzed. The sampling frequency is 25600 Hz and the sampling time is 15 s. The acceleration signal collected by the vertical acceleration sensor with adding noise whose SNB is -2dB is used for the test analysis. And its time domain diagram and the theoretical value curve of IFF are shown in Figs. 16 (a), (b), respectively.

The time-frequency energy distribution based on the FRSST, VMD-SST, PSST and PCT algorithms are shown in Fig. 17. The time-frequency concentrations of the FRSST, VMD-SST, PSST and PCT are analyzed by the Renyi entropy, and the results are shown in Table 5.

TABLE 5. The Renyi entropy.

Algorithms	Renyi entropy
FRSST	19.8761
VMD-SST	23.4685
PSST	22.4091
PCT	23.4875

According to the comparison in Table 5 and Fig. 17, it can be seen that FRSST algorithm has good noise immunity and the time-frequency concentration of the FRSST is the highest. The anti-noise performance of PCT algorithm is higher than that of VMD-SST, but the time-frequency concentration is
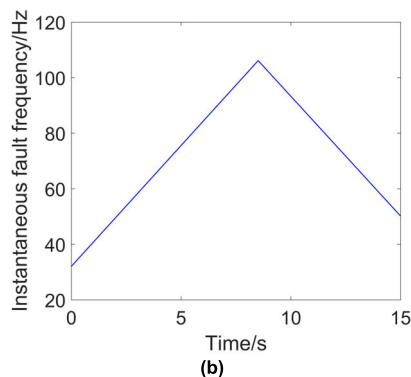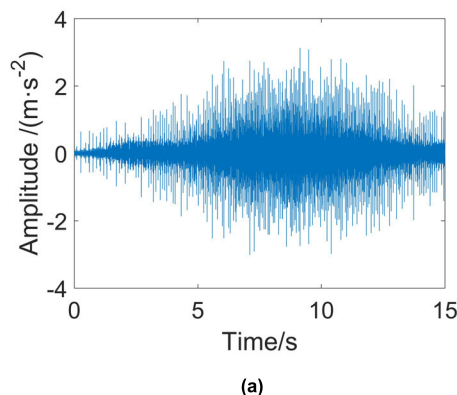

(a)

(b)

FIGURE 16. The signal preprocessing results for actual signals: (a) Time domain diagram; (b) Instantaneous fault frequency curve.

poor. The PSST algorithm is a combination of the PCT and the SST algorithm, so it not only keeps the good anti-noise performance of the PCT algorithm, but also improves the time-frequency concentration. But comparing Table 3 and Table 5, we can get that the Renyi entropy of the FRSST for a rolling bearing with fluctuated speed is larger than the Renyi entropy of the FRSST for a rolling bearing with rising speed. So the FRSST is more suitable for estimating IFF of a rolling bearing with uniform acceleration.

Through theoretical analysis and experimental verification, it can be seen that FRSST algorithm has high accuracy in instantaneous frequency estimation of a rolling bearing with uniform change speed, and as the algorithm of instantaneous frequency estimation, FRSST can also be widely used in rotating machinery in manufacturing industry, sound signals, radar signals and so on. However, for the rotating machinery with complex rotating speed, the algorithm still needs to be improved. The future research on FRSST under complex speed is mainly divided into two categories. One is that multiple LFM signals are used to approximate vibration signals under complex rotating speed which has been studied by more and more scholars, and FRSST is used to estimate the instantaneous frequency. The other is to use the local information characteristics of the signal to study the variable window length adaptive FRSST algorithm, the signal in the appropriate window length range presents linear, so the instantaneous frequency estimation accuracy of a rolling bearing under
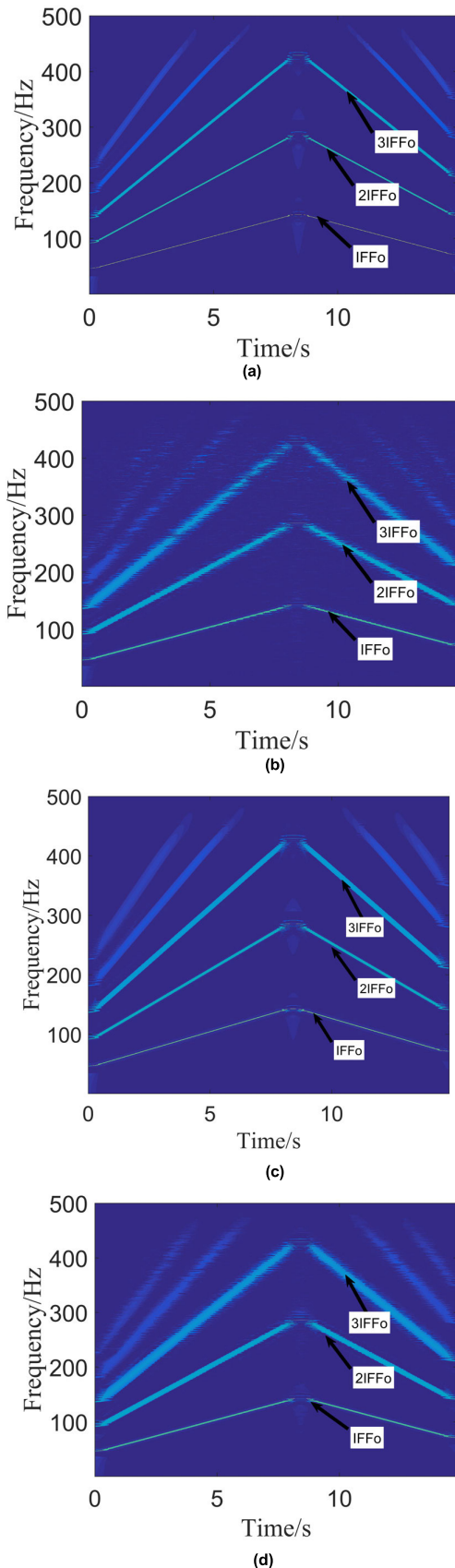
FIGURE 17. Instantaneous time-frequency representations: (a) FRSST; (b) VMD-SST; (c) PSST; (d) PCT.

complex speed is improved. The second category will be our next research work.

VI. CONCLUSION

To improve the accuracy of the IF estimation and the energy concentration of the time-frequency distribution for a multicomponent strong frequency modulation signal, the time-frequency analysis method of the FRSST is proposed. First, the signal with the largest energy is extracted by the STFRFT, and its time-frequency energy distribution is obtained by the SST. Second, because the vibration signals of the rolling bearing are mostly multicomponent signals, the time-frequency distribution of each component signal is obtained by iterative processing. Finally, the time-frequency energy distribution of a multicomponent signal is obtained by superposing the distribution of each component signal. Using the proposed algorithm, the instantaneous frequencies of the simulation signals with different frequency modulation rates, different SNRs and cross-frequency are extracted, as is the IFF of the fault signal. The study draws the following main conclusions:

A. THE HIGH TIME-FREQUENCY CONCENTRATION OF THE FRSST

Compared with the SST, VMD-SST and PSST, the FRSST improves the energy concentration of the time-frequency distribution greatly. For simulation signals, the Renyi entropies of the SST, VMD-SST and PSST increase with the increase of the frequency modulation rate, and the time-frequency concentrations decrease. However, the Renyi entropy of the FRSST does not change much, and the time-frequency concentration is higher than the SST, VMD-SST and PSST.

B. NON-FRAGILE OF THE FRSST TO THE FREQUENCY MODULATION RATE

By the simulation of the signal with a different frequency modulation rate, it can be seen that with the increase of the frequency modulation rate, the estimation error of the instantaneous frequency based on the VMD-SST and PSST increases gradually. The estimation error based on the FRSST is less than the estimations errors of the VMD-SST and PSST, and the error variation amplitude changes little with the increase of the frequency modulation rate. Thus, the FRSST is non-fragile to the frequency modulation rate.

C. NOISE ROBUSTNESS OF THE FRSST

With the increase of the input SNR, the improvement of the SNR of the FRSST is more than the corresponding improvement of the VMD-SST and PSST. Hence, it can be seen that the FRSST has strong noise robustness and is more suitable for practical engineering applications.

D. NONSENSITIVITY OF THE FRSST TO THE CROSS-FREQUENCY SIGNAL

The time-frequency energy of the VMD-SST and PSST at the intersection is divergent, and the instantaneous frequency is marred by confusion and ambiguity. In addition,

the accuracy of the instantaneous frequency estimation based on the FRSST is still better than the corresponding accuracies for the VMD-SST and PSST for a cross-frequency signal.

E. THE FRSST ALGORITHM IMPROVES THE ACCURACY OF THE IFF ESTIMATION

The FRSST algorithm is applied to extract the IFF of a rolling bearing under rising speed and fluctuated speed. Compared with the VMD-SST and PSST algorithms under rising speed, the estimation error of IFF based on the FRSST method is the least for the four fault types. On average, the estimation error is 2.2180 Hz less than the corresponding error of the VMD-SST and 1.1862 Hz less than the corresponding error of the PSST method.

APPENDIX

Acronyms are used in the paper. To facilitate the readers to read the paper, acronyms are listed in the following table in the order they are encountered.

Acronym	The complete spelling
SST	synchrosqueezing transformation
IF	instantaneous frequency
FRSST	Fractional synchrosqueezing transformation
VMD-SST	SST based on variational mode decomposition
PSST	generalized parametric SST
PCT	polynomial chirplet transform
STFT	short-time Fourier transform
WVD	Wigner-Ville distribution
VMD	variational mode decomposition
HV-SST	horizontal–vertical synchrosqueezing transformation
STFRFT	short-time fractional Fourier transform
TSST	time-reassigned synchrosqueezing transformation
LFM	linear frequency modulation
FRFT	fractional Fourier transform
FFT	fast Fourier transform
IFF	instantaneous failure frequency

REFERENCES

[1] B. Ju, H. Zhang, Y. Liu, F. Liu, S. Lu, and Z. Dai, "A feature extraction method using improved multi-scale entropy for rolling bearing fault diagnosis," *Entropy*, vol. 20, no. 4, p. 212, Mar. 2018.

[2] A. Glowacz, W. Glowacz, Z. Glowacz, and J. Kozik, "Early fault diagnosis of bearing and stator faults of the single-phase induction motor using acoustic signals," *Measurement*, vol. 113, pp. 1–9, Jan. 2018.

[3] Y. Liu, Z. Jiang, H. Haizhou, and J. Xiang, "Asymmetric penalty sparse model based cepstrum analysis for bearing fault detections," *Appl. Acoust.*, vol. 165, Aug. 2020, Art. no. 107288.

[4] C. Huang, H. Song, W. Lei, Z. Niu, and Y. Meng, "Instantaneous amplitude-frequency feature extraction for rotor fault based on BEMD and Hilbert transform," *Shock Vib.*, vol. 2019, pp. 1–19, Mar. 2019.

[5] Y. Gao, D. Yu, and H. Wang, "Fault diagnosis of rolling bearings using weighted horizontal visibility graph and graph Fourier transform," *Measurement*, vol. 149, Jan. 2020, Art. no. 107036, doi: 10.1016/j.measurement.2019.107036.

[6] S. Wang, X. Chen, I. W. Selesnick, Y. Guo, C. Tong, and X. Zhang, "Matching synchrosqueezing transform: A useful tool for characterizing signals with fast varying instantaneous frequency and application to machine fault diagnosis," *Mech. Syst. Signal Process.*, vol. 100, pp. 242–288, Feb. 2018.

[7] J. Wen, J. Weng, C. Tong, C. Ren, and Z. Zhou, "Sparse signal recovery with minimization of 1-Norm minus 2-Norm," *IEEE Trans. Veh. Technol.*, vol. 68, no. 7, pp. 6847–6854, Jul. 2019.

[8] J. Wen, L. Li, X. Tang, and W. H. Mow, "An efficient optimal algorithm for the successive minima problem," *IEEE Trans. Commun.*, vol. 67, no. 2, pp. 1424–1436, Feb. 2019.

[9] A. Parey and A. Singh, "Gearbox fault diagnosis using acoustic signals, continuous wavelet transform and adaptive neuro-fuzzy inference system," *Appl. Acoust.*, vol. 147, pp. 133–140, Apr. 2019.

[10] S. Schmidt, P. S. Heyns, and J. P. de Villiers, "A novelty detection diagnostic methodology for gearboxes operating under fluctuating operating conditions using probabilistic techniques," *Mech. Syst. Signal Process.*, vol. 100, pp. 152–166, Feb. 2018.

[11] P. Wang, T. Wang, L. Zhang, and H. Qiao, "Fault diagnosis of rotating machinery under time-varying speed based on order tracking and deep learning," *J. Vibroengineering*, vol. 22, no. 2, pp. 366–382, Mar. 2020.

[12] J. Wu, Y. Zi, J. Chen, and Z. Zhou, "Fault diagnosis in speed variation conditions via improved tacholess order tracking technique," *Measurement*, vol. 137, pp. 604–616, Apr. 2019.

[13] Z. Chen, W. Zhai, and K. Wang, "Vibration feature evolution of locomotive with tooth root crack propagation of gear transmission system," *Mech. Syst. Signal Process.*, vol. 115, pp. 29–44, Jan. 2019.

[14] L. Wang and J. Xiang, "A two-stage method using spline-kernelled chirplet transform and angle synchronous averaging to detect faults at variable speed," *IEEE Access*, vol. 7, pp. 22471–22485, 2019.

[15] Z. Ma, F. Lu, S. Liu, and X. Li, "An adaptive generalized demodulation method for multimedia spectrum analysis is applied in rolling bearing fault diagnosis," *IEEE Access*, vol. 8, pp. 20687–20699, 2020.

[16] D. Zhao, J. Li, W. Cheng, and W. Wen, "Compound faults detection of rolling element bearing based on the generalized demodulation algorithm under time-varying rotational speed," *J. Sound Vib.*, vol. 378, pp. 109–123, Sep. 2016.

[17] X. W. Chen, Z. P. Feng, and M. Li, "Planetary gearbox fault diagnosis under time-variant conditions based on iterative generalized synchrosqueezing transform," *J. Mech. Eng.*, vol. 51, no. 1, pp. 131–137, Oct. 2014.

[18] D. Zhao, T. Wang, R. X. Gao, and F. Chu, "Signal optimization based generalized demodulation transform for rolling bearing nonstationary fault characteristic extraction," *Mech. Syst. Signal Process.*, vol. 134, Dec. 2019, Art. no. 106297, doi: 10.1016/j.ymssp.2019.106297.

[19] D. Liu, W. Cheng, and W. Wen, "Rolling bearing fault diagnosis via ConceFT-based time-frequency reconfiguration order spectrum analysis," *IEEE Access*, vol. 6, pp. 67131–67143, 2018.

[20] G. Yu, "A concentrated time–frequency analysis tool for bearing fault diagnosis," *IEEE Trans. Instrum. Meas.*, vol. 69, no. 2, pp. 371–381, Feb. 2020.

[21] L. Bo, G. Xu, X. Liu, and J. Lin, "Bearing fault diagnosis based on subband time-frequency texture tensor," *IEEE Access*, vol. 7, pp. 37611–37619, 2019.

[22] M. K. Liu and P. Y. Weng, "Fault diagnosis of ball Bearing elements: A generic procedure based on time-frequency analysis," *Meas. Sci. Rev.*, vol. 19, no. 4, pp. 185–194, Aug. 2019.

[23] L. Wang, J. Xiang, and Y. Liu, "A time–frequency-based maximum correlated kurtosis deconvolution approach for detecting bearing faults under variable speed conditions," *Meas. Sci. Technol.*, vol. 30, no. 12, Sep. 2019, Art. no. 125005.

[24] Y. Liu, Z. Jiang, and J. Xiang, "An adaptive cross-validation thresholding de-noising algorithm for fault diagnosis of rolling element bearings under variable and transients conditions," *IEEE Access*, vol. 8, pp. 67501–67518, 2020.

[25] S. C. Amstrup, T. L. McDonald, and G. M. Durner, "Using satellite radiotelemetry data to delineate and manage wildlife populations," *Wildlife Soc. Bull.*, vol. 32, no. 3, pp. 661–679, Sep. 2004.

[26] T. A. C. M. Claasm and W. F. G. Mecklenbrauker, "The wigner distribution-a tool for time-frequency signal analysis," *Philips J. Res.*, vol. 35, nos. 4–5, pp. 276–300, 1980.

[27] S. Liu, Y. D. Zhang, T. Shan, and R. Tao, "Structure-aware Bayesian compressive sensing for frequency-hopping spectrum estimation with missing observations," *IEEE Trans. Signal Process.*, vol. 66, no. 8, pp. 2153–2166, Apr. 2018.

[28] I. Daubechies, J. Lu, and H. T. Wu, "Synchrosqueezed wavelet transforms: An empirical mode decomposition-like tool," *Appl. Comput. Harmon. Anal.*, vol. 30, no. 2, pp. 243–261, Mar. 2011.

[29] G. Thakur and H.-T. Wu, "Synchrosqueezing-based recovery of instantaneous frequency from nonuniform samples," *SIAM J. Math. Anal.*, vol. 43, no. 5, pp. 2078–2095, Jan. 2011.

[30] C. Li and M. Liang, "Time–frequency signal analysis for gearbox fault diagnosis using a generalized synchrosqueezing transform," *Mech. Syst. Signal Process.*, vol. 26, pp. 205–217, Jan. 2012.

[31] D. Abboud, J. Antoni, S. Sieg-Zieba, and M. Eltabach, "Envelope analysis of rotating machine vibrations in variable speed conditions: A comprehensive treatment," *Mech. Syst. Signal Process.*, vol. 84, pp. 200–226, Feb. 2017.

[32] Z. Ma, W. Ruan, M. Chen, and X. Li, "An improved time-frequency analysis method for instantaneous frequency estimation of rolling bearing," *Shock Vib.*, vol. 2018, pp. 1–18, Sep. 2018, doi: 10.1155/2018/8710190.

[33] I. Daubechies, Y. Wang, and H.-T. Wu, "ConceFT: Concentration of frequency and time via a multitapered synchrosqueezed transform," *Phil. Trans. Roy. Soc. A, Math., Phys. Eng. Sci.*, vol. 374, no. 2065, Apr. 2016, Art. no. 20150193, doi: 10.1098/rsta.2015.0193.

[34] Q. Li, M. J. Zuo, and C. Cattani, "Bearing fault diagnosis using sparse Daubechies-wavelet impulse isolation and horizontalŬvertical synchrosqueezing transform approach," *ISA Trans.*, to be published, doi: 10.1016/j.isatra.2020.02.002.

[35] K. Yu, Z. T. Luo, H. F. Li, and H. Ma, "General parameterized synchrosqueezing transform and its application in rotating machinery vibration signal," *J. Mec. Eng.*, vol. 55, no. 11, pp. 149–159, Jun. 2019.

[36] Y. Yang, Z. K. Peng, X. J. Dong, W. M. Zhang, and G. Meng, "General parameterized time-frequency transform," *IEEE Trans. Signal Process.*, vol. 62, no. 11, pp. 2752–2764, Mar. 2014.

[37] D. He, H. Cao, S. Wang, and X. Chen, "Time-reassigned synchrosqueezing transform: The algorithm and its applications in mechanical signal processing," *Mech. Syst. Signal Process.*, vol. 117, pp. 255–279, Feb. 2019.

[38] H. Cao, X. Wang, D. He, and X. Chen, "An improvement of time-reassigned synchrosqueezing transform algorithm and its application in mechanical fault diagnosis," *Measurement*, vol. 155, Apr. 2020, Art. no. 107538, doi: 10.1016/j.measurement.2020.107538.

[39] Y. Zhang, X. Du, G. Wen, X. Huang, Z. Zhang, and B. Xu, "An adaptive method based on fractional empirical wavelet transform and its application in rotating machinery fault diagnosis," *Meas. Sci. Technol.*, vol. 30, no. 3, Mar. 2019, Art. no. 035005, doi: 10.1088/1361-6501/aaf8e6.

[40] J. Mei, J. Jia, R. Zeng, B. Zhou, and H. Zhao, "A multi-order FRFT self-adaptive filter based on segmental frequency fitting and early fault diagnosis in gears," *Measurement*, vol. 91, pp. 532–540, Sep. 2016.

[41] H. Q. Wang, "Fractional S transform and its application to gearbox fault diagnosis," *J. Elec. Meas. Instru.*, vol. 33, no. 8, pp. 133–139, Aug. 2019.

[42] H. Zhang, T. Shan, S. Liu, and R. Tao, "Optimized sparse fractional Fourier transform: Principle and performance analysis," *Signal Process.*, vol. 174, Sep. 2020, Art. no. 107646.

[43] L. Li and D. Li, "Exact solutions and numerical study of time fractional Burgers' equations," *Appl. Math. Lett.*, vol. 100, Feb. 2020, Art. no. 106011, doi: 10.1016/j.aml.2019.106011.

[44] D. Li, H.-L. Liao, W. Sun, J. Wang, and J. Zhang, "Analysis of L1-Galerkin FEMs for time-fractional nonlinear parabolic problems," *Commun. Comput. Phys.*, vol. 24, no. 1, pp. 86–103, 2018.

[45] X. Li, Z. Ma, D. Kang, and X. Li, "Fault diagnosis for rolling bearing based on VMD-FRFT," *Measurement*, vol. 155, Apr. 2020, Art. no. 107554, doi: 10.1016/j.measurement.2020.107554.

[46] H. Hao, "Multi component LFM signal detection and parameter estimation based on EEMD–FRFT," *Optik*, vol. 124, no. 23, pp. 6093–6096, Dec. 2013.

[47] S. A. Elgamel and J. J. Soraghan, "Using EMD-FrFT filtering to mitigate very high power interference in chirp tracking radars," *IEEE Signal Process. Lett.*, vol. 18, no. 4, pp. 263–266, Apr. 2011.

[48] J. B. Luan and B. Deng, "Time-frequency resolving ability of short-time fractional Fourier transform to FM signals," *Telecommun. Eng.*, vol. 55, no. 7, pp. 773–778, Jul. 2015.

[49] A. J. Hu and Y. Zhu, "Instantaneous frequency estimation of a rotating machinery based on an improved peak search method," *J. Vib. Shock*, vol. 32, no. 7, pp. 113–117, Apr. 2013.

[50] D.-Z. Zhao, J.-Y. Li, W.-D. Cheng, T.-Y. Wang, and W.-G. Wen, "Rolling element bearing instantaneous rotational frequency estimation based on EMD soft-thresholding denoising and instantaneous fault characteristic frequency," *J. Central South Univ.*, vol. 23, no. 7, pp. 1682–1689, Jul. 2016.

[51] J. Shi, M. Liang, D.-S. Necsulescu, and Y. Guan, "Generalized stepwise demodulation transform and synchrosqueezing for time–frequency analysis and bearing fault diagnosis," *J. Sound Vib.*, vol. 368, pp. 202–222, Apr. 2016.

XIN LI received the B.S. degree from Liaoning Shihua University, in 2012, and the M.S. degree from Northeastern University, in 2014. She is currently pursuing the Ph.D. degree with Shijiazhuang Tiedao University. Her main research interests include rotating machinery condition monitoring and fault diagnosis.

ZENGQIANG MA received the Ph.D. degree from Beijing Jiaotong University, China, in 2011.

He is currently the Special Allowance Expert of the Hebei Provincial Government, the second-level talent of the 333 talent project in Hebei, a member of the Steering Committee of Electrical Information Teaching, Hebei Higher Education Institutions, and the Director of the Hebei Electrotechnical Society. He is also a Ph.D. Supervisor and the Deputy Dean of the School of Electrical and Electronic Engineering, Shijiazhuang Tiedao University. He mainly researches the field of safety operation state monitoring and fault diagnosis of rail vehicles, takes the fault or damage identification of wheelset bearings, treads, rails, pantographs, catenaries, and other equipment that affect the safety of rail transit vehicles as research directions. His works based on digital signal processing, digital image processing, embedded development, and other technologies, carrying out algorithm innovation, system simulation, experimental verification, and prototype development.

SUYAN LIU (Member, IEEE) received the Ph.D. degree from the Beijing University of Posts and Telecommunications, China, in 2019. She worked as a Software Engineer for Six years and became a Senior Computer Engineer, in 2015. She is currently a Lecturer with the School of Shijiazhuang Tiedao University, China. Her current research interests include machine learning, the Internet of Things, and multimedia image processing technology for fault diagnosis of rolling bearing.

FEIYU LU received the B.S. degree from Beihua University, in 2018. He is currently pursuing the M.S. degree with Shijiazhuang Tiedao University. His main research interests include rotating machinery condition monitoring and fault diagnosis.

● ● ●